Volume 1 | Number 1 | Jan 2013 | Pages 1–100

PCCP

Physical Chemistry Chemical Physics
www.rsc.org/pccp

ROYAL SOCIETY OF CHEMISTRY

ROYAL SOCIETY OF CHEMISTRY

www.rsc.org/pccp

"On the Ag^{+}-Cytosine interaction: effect of microhydration probed by IR optical spectroscopy and density functional theory"

Matias Berdakin,[1] Vincent Steinmetz,[2] Philippe Maitre[2] and Gustavo A. Pino[1]*

1) INFIQC (CONICET – Universidad Nacional de Córdoba). Dpto. de Fisicoquímica – Facultad de Ciencias Químicas – Centro Láser de Ciencias Moleculares – Universidad Nacional de Córdoba, Ciudad Universitaria, X5000HUA Córdoba, Argentina

2) Laboratoire de Chimie Physique – Université Paris Sud – UMR8000 CNRS – Faculté des Sciences – 91405 Orsay Cedex – France.

*Corresponding author: gpino@fcq.unc.edu.ar

Abstract

The gas-phase structures of cytosine-Ag$^+$ [CAg]$^+$ and cytosine-Ag$^+$-H$_2$O [CAg-H$_2$O]$^+$ complexes have been studied by mass-selected infrared multiphoton dissociation (IRMPD) spectroscopy in the 900 – 1800 cm^{-1} spectral region with the Free Electron Laser facility in Orsay (CLIO). The IRMPD experimental spectra have been compared with the calculated IR absorption spectra of the different low-lying isomers (computed at the DFT level using the B3LYP functional and the 6-311G++(d,p) basis set for the C, H, N and O atoms and the Stuttgart effective core potential for Ag).   For the [CAg]$^+$ complex, only one isomer with cytosine in the keto-amino (KA) tautomeric form and Ag$^+$ interacting simultaneously with the C(2)=O(7) group and N(3) of cytosine, was observed.   However, the mono-hydration of the complex in the gas phase leads to the stabilization a two quasi-isoenergetic structures of the [CAg-H$_2$O]$^+$ complex, in which Ag$^+$ interacts with the O atom of the water molecule and with N(3) or C(2)=O(7) group of cytosine. The relative populations of the two isomers determined from the IRMPD kinetics plot are in good agreement with the calculated values. Comparison of these results with those of protonated cytosine [CH]$^+$ and its mono-hydrated complex [CH-H$_2$O]$^+$, shows some interesting differences between H$^+$ and Ag$^+$. In particular, while a single water molecule catalyzes the isomerization reaction in the case of [CH-H$_2$O]$^+$, it is found that in the case of [CAg-H$_2$O]$^+$ the addition water lead to the stabilization of two isomers separated by small energy barrier (0.05 eV).

1. Introduction

DNA, a fundamental molecule in nature, is composed of four building blocks Adenine (A), Thymine (T), Guanine (G) and Cytosine (C) that constitute the alphabet of the genetic code. In the canonical form they form two complementary pairs A-T and G-C through specific hydrogen bonds (H-bonds) patterns, known as the Watson-Crick (WC) pairs. This recognition is a key for the correct transfer of the genetic information.[1]

It is well established that metal cations binding to the DNA bases can induce the formation of rare tautomers, with different hydrogen bonding patterns to those required for the molecular recognition of the WC pairs.[2,3] In this sense, in the last years there has been an increasing interest in developing non-conventional DNA base pairs, by replacing one H involved in a H-bond by a metal cation.[4] Besides, the incorporation of metal mediated base pairing has proven to be a suitable and powerful tool for the potential development of artificial DNA based devices[5,6] due to the robustness and rigidity of the DNA to form nanostructures and the remarkable biorecognition capability of this molecule.

The interaction of transition metal cations with DNA bases is highly specific, for instance the T-T and C-C mismatch pairs can be transformed into very stable T-Hg^{2+}-T[7] and C-Ag^+-C[8,9] metallo-mediated base pairs, by incorporating Hg^{2+} or Ag^+ cations, respectively, with a very strong metal-base interactions.

These interesting characteristics have been inspiration for conducting experimental studies of the DNA bases-metal cations interactions in the gas phase from a molecular level, to allow a direct correlation between experiments and in-vacuo *ab initio*/DFT and get information on the effects of these interactions on the intrinsic physical and chemical properties of the bases. Vibrational (Infrared) and electronic (UV-vis) photofragmentation spectroscopy of mass-selected ions, coupled to tandem mass spectrometry has become a powerful tool for studying the structure, reactivity and excited state dynamics of cationized molecules and the DNA bases and their dimers.

Since the development of soft ionizations sources such as Electrospray Ionization (ESI), ionizing a base through addition of H$^+$ is a quite straightforward procedure and therefore, gas phase spectroscopy of protonated DNA bases has been broadly studied. In this sense, the gas phase infrared multiphoton spectroscopy (IRMPD) of the three pyrimidine bases, Cytosine (C), Uracil (U) and Thymine (T)[10-12] as well as the UV electronic spectroscopy of the five DNA/RNA bases,[13-16] have been reported. In recent works, detailed experimental studies of the proton mediated homo-dimers of cytosine,[17,18] substituted cytosines[19-21] tymine,[18] uracile[18] and adenine[22] have been conducted.

Less attention has been paid to the gas phase spectroscopy, structure, binding energies and optical properties of DNA bases-metal cation complexes in spite of the importance of these interactions as mentioned above. The gas phase structures of the 1:1 complexes between alkali metal cations-Cytosine,[23] Na$^+$-Halo-Uraciles,[24] Pb^{2+}-Uridine 5´-monophosphate,[25] Pb^{2+}-cytidine 5-monophosphate and Pb^{2+}-deoxycytidine 5-monophosphate,[26] Cisplatin-Adenine/Guanine,[27] Pb^{2+}-deprotonated 2-deoxyguanosine 5'-monophsphate,[28] and metal-mediated Hoogsteen-type base pairs[29]. have been determined by means of mass selected IRMPD spectroscopy in combination with quantum chemical approaches. Extensive theoretical work has also been conducted to address this problem, in which comparisons between binding metal neutral atoms, metal cations and metal anions to DNA bases[30-32] as well a small metal clusters[33-36] have been pointed out.

Recently, the structure of the (Cytosine)$_2$Ag$^+$ [C$_2$Ag]$^+$ complex has been determined by the same methodology[37] and it was shown that it mimics the structure of the hemiprotonated [C$_2$H]$^+$ dimer responsible for the stabilization of the *i*-motif structure in DNA, with the replacement of the NH…N bond by a stronger N…Ag$^+$…N bond, which is in line with the recent findings of *i*-motif formation at neutral pH in presence of Ag$^+$ cations.[38] Such result is surprising since H$^+$ and Ag$^+$ are quite different in size which makes H$^+$ and Ag$^+$ behaves as a hard and soft acid, respectively but in the case of the [C$_2$Ag]$^+$ and [C$_2$H]$^+$ complexes, their structural influences are similar. However, the effects of H$^+$ and Ag$^+$ on the electronic

excited state properties of both complexes are remarkably different. The excited state lifetime of $[C_2H]^+$

(τ = 85 fs) is at least two orders of magnitude shorter than that of $[C_2Ag]^+$ (τ > 5300 fs).[39]

While in the two complexes $[C_2Ag]^+$ and $[C_2H]^+$, both cytosine molecules are found in the

canonical keto-amino (KA) tautomeric form, previous works have shown that protonation of a single C

molecule $[CH]^+$ also stabilizes a rare enol-amino (EA) tautomer in addition to the canonical KA

tautomer[10,13] and both structures are also stabilized by interaction with a single water molecule on the

protonation site.[12] This fact motivated us to study the effects of replacing the H^+ in $[CH]^+$ by Ag^+ in $[CAg]^+$

in order to address the following question:

    i) Does Ag^+ also induce the stabilization of rare tautomers of cytosine in the gas phase?

    ii) What is the preferred interacting site for Ag^+?

    iii) What is the effect of a single water molecule on the structure of the $[CAg]^+$ complex?

    iv) Where is the preferred interaction position of H_2O?

Therefore, we report here a study on the IRMPD spectroscopy of the mass selected $[CAg]^+$ and

$[CAg-H_2O]^+$ complexes in the gas phase together with quantum-chemical calculations.

2. Methodology

2.a. IR-MPD Spectroscopy

The IR-MPD spectra of $[CAg]^+$ and $[CAg-H_2O]^+$ complexes were obtained with the tunable IR

radiation from the Free Electron Laser (IR-FEL) and the CO_2 laser available at CLIO, coupled to a modified

FT-ICR (7T FT-ICR Bruker Apex Qe) with an electrospray ionization (ESI) source. The coupling of the laser

system with the ICR cell has already been described in detail elsewhere.[40]

A 25 µM $AgNO_3$ and 50 µM cytosine solution was prepared in a 1:1 of water:methanol mixture

and introduced into the ESI source to generate $[CAg]^+$ and $[CAg-H_2O]^+$ complexes under the following

conditions: flow rates of 150 µL/h, spray voltages of 4000 V, drying gas flow of 4 $L.s^{-1}$, nebulizer

pressures of 1.5 bar and drying gas temperature of 150 ºC. All the reactants were obtained from Sigma-Aldrich and used without further purification.

To obtain the IR-MPD spectra, the parent ion complexes, $[CAg]^+$ and $[CAg-H_2O]^+$, were mass selected in the quadrupole mass stage and subsequently irradiated in the ICR cell. The irradiation conditions were optimized to maximize the fragmentation efficiency of the parent ion of interest. In the case of the $[CAg]^+$, the complex was irradiated under strong irradiation power conditions, namely 3 seconds of IR-FEL at 900 mW and at repetition rate of 40 Hz coupled to 38 ms of the CO_2 laser emission. For the $[CAg-H_2O]^+$ complex milder condition were employed, 100 ms of IR-FEL emission coupled with the 30 ms of the CO_2 laser emission. With the FEL tuned to a vibrational transition, the ions absorbed multiple IR photons in a stepwise process until the dissociation threshold was reached. By monitoring the intensities of parent (I_{parent}) and resulting fragment ions ($I_{fragment}$) as a function of the laser frequency, the IR-MPD spectrum was obtained as the fragmentation efficiency $Y = - \ln(I_{parent}/[I_{parent} + \Sigma I_{fragment}])$.

2.b. Computational Details

The potential energy surfaces of the $[CAg]^+$ and $[CAg-H_2O]^+$ complexes were explored at the DFT theory level with the B3LYP functional and using the 6-311G++(d,p) basis set for the C, H, N and O atoms and the Stuttgart effective core potential for Ag.[41] In the case of the $[CAg-H_2O]^+$ two closely resembling structures were determined as energy minima, therefore, further levels of theory were employed to rule out the possibility that the existence of both structures were an artifact of the calculations. In this case, both structures were optimized with the B3LYP and M062X functionals and using both the Stuttgart[41] and the Radloff[42] effective core potential to describe the silver cation.

Spectral assignment was achieved by comparing experimental spectra and calculated IR absorption spectra. The IR linear absorption spectra of each minimum of energy structures were computed at the B3LYP level of theory. Despite the multiphotonic nature, the IRMPD spectrum

predominantly reflects the absorption of the first IR photon, which justifies its comparison with the calculated linear one-photon IR absorption spectrum.

The IRMPD line width intrinsically depends on the finite laser bandwidth of 0.5% of the central wavelength (corresponding to Δv = 5.0 − 10.5 cm^{-1} for v = 1000 − 2000 cm^{-1}), the unresolved rotational structure and, to a lesser extent, on the spectral broadening arising from the multiphotonic character of the IR-MPD process. For the sake of comparison, calculated bands were convoluted assuming a Lorentzian profile with 10 cm^{-1} full width at half maximum (FWHM).

Finally, the relative Gibbs free energies (ΔG) were computed at the same level of theory, at 300 K. Following the mass-selection in a quadrupole, the ions are thermalized at 300 K in a linear hexapole filled with argon bath gas prior to the transfer to the low-pressure ICR cell.[43]

All calculations were performed using the Gaussian09 program package.[44]

3. Results and Discussion

3.a. The [CAg]$^+$ Complex
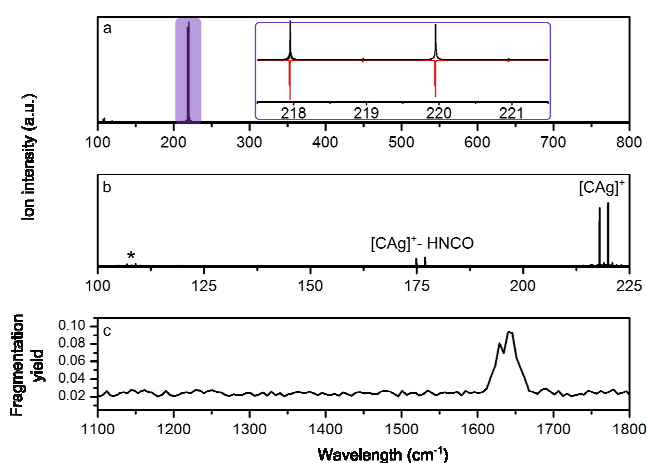
A typical positive-ion mass spectrum after selection of the [C+Ag]$^+$ ion (m/z = 217.8 and 219.8) with the characteristic isotopic pattern of this specie is shown in Figure 1.a, together with the simulated isotopic distribution.

Figure 1.b shows the mass spectrum obtained when the [CAg]$^+$ complex is irradiated with 1640 cm^{-1} photons. The only product observed corresponds to the loss of a neutral fragment of 43 a.m.u., most probably due to the elimination of the isocianic acid group (HNCO) of cytosine. The presence of the Ag$^+$ (indicated as *) is depicted in the same figure. The intensity of the signal correspondent to Ag$^+$ is independent on the irradiation wavelength (Figure S1.a), so it was not taken into account for the calculation of the fragmentation efficiency. The fragmentation channel observed for [CAg]$^+$ is rather

unexpected considering that in the case of the [C-Alkali Metal]⁺ IRMPD induces the loss of the neutral cytosine molecule.[23]

The IRMPD spectrum of the [CAg]⁺ complex obtained considering the only fragmentation product observed (Figure 1.c) was acquired under strong irradiation conditions as described in the experimental section. Despite the strong irradiation conditions, the fragmentation yield obtained was low, reaching 8 % with the laser tuned at 1643 cm⁻¹, on the top of the single experimental band observed, which is lower than the fragmentation yield reported for the complexes [C-Alkali Metal]⁺, ranging 16 - 100 %, for M⁺= Li⁺ and Cs⁺, respectively at softer irradiation conditions.[23]

Figure 1. (a) Typical mass spectrum of the isolated [CAg]⁺ complex obtained infusing a solution of 25 μM AgNO₃ and 50 μM cytosine prepared in a 1:1 water:methanol mixture. The inset of the figure shows a zoom in on the parent ion signal (black line) and the simulated isotopic distribution (red line) that reinforce the identification of the species. (b) Mass spectrum obtained when the [CAg]⁺ complex is irradiated with 1640 cm⁻¹ photons. The only product observed corresponds to the loss of the m = 43 a.m.u. neutral fragment. In both (a) and (b) the presence of the silver cation is depicted with (*). (c) IRMPD spectrum obtained between 1100 cm⁻¹ and 1800 cm⁻¹. The irradiation condition in (b) and (c) was 3 seconds of IR-FEL (900 mW and 40 Hz) coupled to 38 ms of the CO₂ laser emission.

The IRMPD spectrum of the [CAg]⁺ complex shows a single broad band centered at 1643 cm⁻¹ that closely resembles that of the [CLi]⁺ complex[23] which presents two broad bands around 1635 cm⁻¹

and 1480 cm^{-1}, although the fragmentation yield of the latter is higher. For the heavier alkali cations, the fragmentation yields are higher and more spectral features were found, while the band peaking at 1635 cm^{-1} is considerably blue shifted as the size of the metal increases.[23]

To aid in the interpretation of the observed spectrum and bring information about the complex structure, DFT calculations were performed as was described in section 2.b. A targeted exploration of the potential energy surface was carried out, and multiple trial structures were considered for the geometry optimization. The starting structures were based on different tautomers of cytosine (keto (K), enol (E), amino (A), imino (I)) and different σ- or π-type bonding motifs of Ag$^+$ were considered. In order to generate a straightforward nomenclature, the different isomers were labeled employing the tautomeric form of the molecule. In those cases where more than one structure with the same tautomeric state were found, the different isomers were differentiated with integer numbers increasing with the relative energy. Overall, σ-type structures are favored, and the lowest π-type structure is 1.24 eV higher than the lowest energy σ-type structure. As a result, such a binding motif was not taken in to account for the discussion.
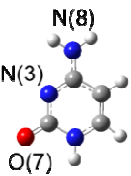
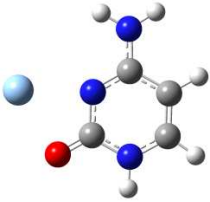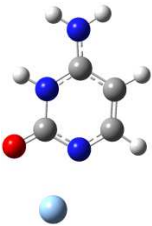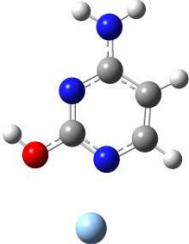The structure of the six most stable isomers spanning all the tautomeric forms of the molecule, in addition to ΔG(300 K), and ΔH(0 K), relative to the most stable isomer and corrected by the zero point energy are given in Table 1. It should be pointed out that, before irradiation the ions are thermalized to near room temperature,[43] thereby the relative population of each isomers (R.P.) was estimated considering a Boltzmann distribution at 300K (Table 1).
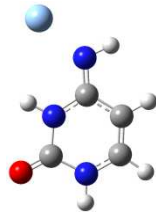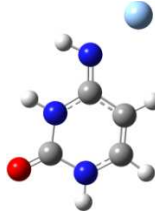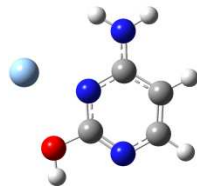
In the calculated minimum energy isomer of [CAg]$^+$, hereafter named KA1, the cytosine molecule presents keto-amino (KA) tautomerism, as in [CM]$^+$ related systems[23] and it interacts with the cation through both, the lone electron pairs of N(3) and the oxygen of the C(2)=O(7) group as reported in a previous theoretical study of the same complex.[32,45] It is well known that neutral cytosine can bind metal ions simultaneously through N(3) and O(7)[3] as already observed in gas phase [C-Alkali metal]$^+$
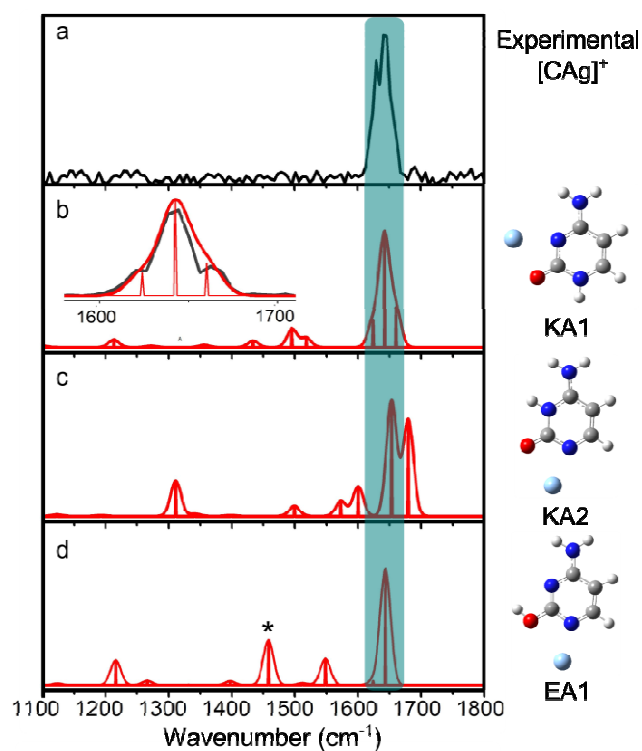
complexes.[23] The second isomer (KA2) is 0.15 eV less stable than KA1 and also presents keto-amino tautomerism but in this case the cation interacts with the lone electros pair of the N(1) and the C(2)=O(7) group. Of the next four isomers, two of them present enol-amino (EA) tautomerism and the other two show keto-imino (KI) tautomerism. Those structures are considerably less stable than the isomers with KA tautomerism, and therefore their R.P. are extremely low and can be neglected.

Structural assignment was based on the comparison of the experimental spectrum (Figure 2.a) with the predicted IR linear absorption spectra of the three lowest energy isomers which are given in Figure 2.(b-d).

Table 1. Most stable isomers of the [CAg]$^+$ complex spanning all the tautomeric forms of the molecule. The potential energy surface was explored at the B3LYP level of theory using the 6-311G++(d,p) basis set for the C, H, N and O atoms and the Stuttgart effective core potential for Ag.[41] Thermochemical properties have been computed at 300K taking in to account the zero point correction. R.P. stands for relative population. All the values are expressed in eV.

	KA1	KA2	EA1
ΔH (0 K)	0	0.15	0.25
ΔG (300 K)	0	0.14	0.25
Relative Population (R.P.)	1 (99.6 %)	4.0×10^{-3} (0.4 %)	5.3×10^{-5}

	KI1	**KI2**	**EA2**
ΔH (0 K)	0.44	0.47	0.52
ΔG (300 K)	0.43	0.45	0.51
Relative Population (R.P.)	5.1x10^{-8}	2.4x10^{-8}	2.7x10^{-9}

Figure 2. a) Experimental IRMPD spectrum of [CAg]$^+$ complex recorded under 3 seconds of IR-FEL (900 mW and 40 Hz) coupled

to 38 ms of the CO$_2$ laser emission. (b-d) Simulated IR absorption spectra of the three most stable isomers. The inset in (b)

exhibits a higher resolution spectrum recorded in the 1600 cm^{-1} – 1700 cm^{-1} spectral region (black) recorded under stronger

irradiation conditions (5 seconds of IR-FEL (900 mW and 40 Hz) coupled to 38 ms of the CO$_2$ laser emission), together with the

simulated spectrum (red).

Figure 2.b presents the IR spectrum of the KA1 isomer. In the region between 1600 cm^{-1} and 1700 cm^{-1} the simulated spectrum shows three transitions at 1624 cm^{-1}, 1639 cm^{-1} and 1660 cm^{-1} that correspond to the NH_2 scissoring, the carbonyl stretching, and a combination mode arising from coupling of the carbonyl stretch, NH_2 scissoring and N1−H wagging, respectively. Due to the low spectral resolution (FWHM = 10 cm^{-1}), the overlap of these three transitions results in a single broad band centered at 1643 cm^{-1}, which fits the experimental spectrum. The inset of Figure 2.b shows a higher resolution spectrum acquired under stronger irradiation conditions (5 seconds of IR-FEL at 900 mW and 40 Hz coupled to 38 ms of the CO_2 laser emission) in the 1600 − 1700 cm^{-1} spectral region. In the experimental spectrum the broad band splits in a central band and two shoulders that are remarkably fitted by the simulated IR absorption spectrum. Figure 2.c exhibits the IR simulated spectrum calculated for the KA2 isomer. The major feature of the spectrum also appears in the 1600 cm^{-1} − 1700 cm^{-1} region, but in this case, the spectrum presents a double intense band caused by the blue shift carbonyl stretch at 1680 cm^{-1}, resulting in a poor agreement with the experimental spectrum. However, in the experimental spectrum (Figure 2.a) there may be a very week band at 1690 cm^{-1}, that could correspond to the KA2 isomer which is expected to be present at lower concentration than the KA1 isomer. Therefore, a weak population of the KA2 isomer cannot be completely ruled out. Finally Figure 2.d shows the simulated IR spectrum of the EA1 isomer, which presents only a narrow band assigned to the NH_2 scissoring mode peaking at 1642 cm^{-1}, in good agreement with the center of the experimental band at 1643 cm^{-1}. Nevertheless, nor the width of the band neither the presence of the two shoulders observed in the inset of Figure 2.b can be accounted for using only this spectrum. Furthermore, a second intense feature is predicted at 1460 cm^{-1} (depicted with *) which corresponds to the in-plane deformation of the ring, however no bands are observed in the experimental spectrum in this spectral region. Finally, the population of this isomer is predicted to be five orders of magnitude lower than the concentrations of the most stable KA1 isomer (Table 1).
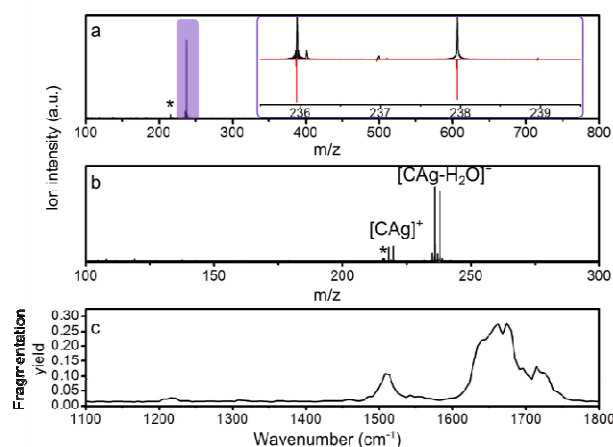
The low fragmentation yield of the complex clearly precludes the possibility of obtaining richer spectroscopic information from less intense bands, and reinforce the assignment with more spectral signatures as in the case of the [CLi]$^+$.[23] Due to the low fragmentation yield in the FEL range, spectroscopy in the OH and NH stretchings region (2500 – 3800) cm^{-1} is very likely to be difficult due to the lower power of the OPO laser as compared to the FEL. Nevertheless, bringing together the prominent fitting of the experimental and simulated spectra of the KA1 isomer, the low relative population of the higher energy isomers, and the fact that in related [CM]$^+$ systems[23] cytosine presents keto-amino (KA) tautomerism, strongly support the conclusion that the KA1 isomer is responsible of the observed IRMPD spectrum.

This is in line with previous theoretical reports[32,45] suggesting that Ag$^+$ does not stabilize rare tautomers but only the canonical KA one, in contrast to H$^+$ that lead to the formation of the protonated KA and EA tautomers, with an energy barrier for the 1,3 proton transfer/isomerization reaction of 157 kJ/mol.[10]

3.c. The [CAg-H$_2$O]$^+$ Complex

A typical positive ion mass spectrum after isolation of the [C+Ag+H$_2$O]$^+$ ion (m/z = 329.8 and 331.8) is shown in Figures 3.a, together with the simulated isotopic distribution. Figure 3.b shows the mass spectrum obtained when the [CAg-H$_2$O]$^+$ complex is irradiated with 1670 cm^{-1} photons. In this case, the only product observed corresponds to the loss of a neutral water molecule. The peak at *m/z* 216 depicted as (*) in Figures 3.a and 3.b, corresponds to an unknown contaminant whose intensity does not show any dependence on the irradiation wavelength (Figure S1.b), so it was not taken in to account for the calculation of the fragmentation efficiency. The IRMPD spectrum of the [CAg-H$_2$O]$^+$complex obtained considering the only fragmentation product observed was acquired under mild condition, as described in the experimental section, in the spectral range (1100 - 1800) cm^{-1} and is shown in Figure 3.c. The most

intense feature of the spectra is a wide band peaking at 1667 cm^{-1} with one shoulder at 1719 cm^{-1} and an unresolved band at 1639 cm^{-1}. In addition, two minor bands are observed at 1511 cm^{-1} and 1215 cm^{-1}. It is important to point out that, the resolution of the broad band centered at 1667 cm^{-1} could not be improved, despite the use of attenuators to reduce the saturation effects due to the irradiation power. This fact seems to indicate that the broad feature obtained could be due to the overlap of more than one vibrational band.

Figure 3. (a) Typical mass spectrum of the isolated [CAg-H$_2$O]$^+$ complex obtained infusing a solution of 25 μM AgNO$_3$ and 50 μM cytosine prepared in a 1:1 water:methanol mixture. The inset of the figure shows a zoom in on the parent ion signal (black line) and the simulated isotopic distribution (red line) that reinforce the identification of the species. (b) mass spectrum obtained when the [CAg-H$_2$O]$^+$ complex is irradiated with 1670 cm^{-1} photons. The only product corresponds observed to the loss of a neutral water molecule. In both (a) and (b) the presence of an unknown specie of mass 216 a.m.u. is depicted with (*). (c) IRMPD spectrum obtained between 1100 cm^{-1} and 1800 cm^{-1}.

To aid in the interpretation of the observed spectrum and bring in information about the structure of the complex, DFT calculations were performed as described in section 2.b. The potential energy surface of the [CAg-H$_2$O]$^+$ complex was explored starting from multiple trial structures. These starting structures were originated considering different binding positions of the water molecule to the KA1 [CAg]$^+$ complex, spanning all functional groups and the silver cation. All the low-energy structures derive from the keto-amino cytosine tautomer. The different resulting isomers were named [CAg-H$_2$O]$^+$-

X, where X is an integer increasing with the relative energy. The optimized structures are displayed in Table 2, together with their corresponding relative ΔG(300 K) and the ΔH(0K). It is worth noting that for this complex no stationary point with π-type $[CAg]^{+\cdots}H_2O$ binding motif could be optimized.

As can be seen in Table 2, the solvation of the $[CAg]^+$ complex is more favorable when the water molecule interacts directly with the silver cation than when it forms a hydrogen bond with a functional group of cytosine. Interestingly, two similar and quasi-isoenergetic structures, hereafter called $[CAg-H_2O]^+$-1 and -2, were determined as energy minima on the potential energy surface. These two isomers are predicted to be populated assuming a Boltzmann population of the isomers (see Table 2).
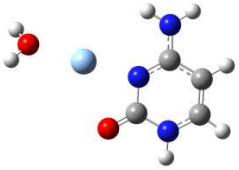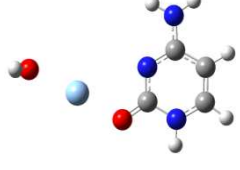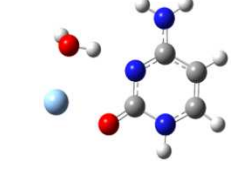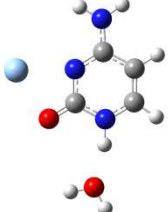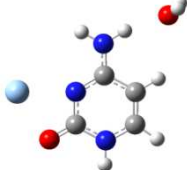
In the $[CAg-H_2O]^+$-1 lowest energy structure, the silver cation binds to the N(3) of cytosine and to the O atom of the water molecule. Interestingly, a typical linear dicoordination with a calculated O-Ag^+-N(3) angle of 180° is predicted. In the $[CAg-H_2O]^+$-2 isomer, the Ag^+ cation is bound to the carbonyl oxygen of cytosine and the water oxygen, and the O-Ag^+-O angle is predicted to be 180°. This common feature between the mentioned structures is expected given that Ag^+ is well known to preferentially form di-ligated complex through linear coordination.[46,47] As mentioned in the method section, additional simulations were performed in order to ascertain the existence of these two minima on the potential energy surface. Both structures were re-optimized with the B3LYP and M062X functional and using both the Stuttgart[41] and the Radloff[42] effective core potential to describe the silver cation. The obtained structures and energetics are summarized in Table S1. It is found that structures $[CAg-H_2O]^+$-1 and $[CAg-H_2O]^+$-2 remain as energy minima for the $[CAg-H_2O]^+$ system at all level of theory.

Higher energy isomers have been characterized, such as $[CAg-H_2O]^+$-3, $[CAg-H_2O]^+$-4, and $[CAg-H_2O]^+$-5 shown in Table 2. In $[CAg-H_2O]^+$-3 structure, the water molecule acts simultaneously both as an electron donor to Ag^+ and a hydrogen bond donor to cytosine N(3). Structures $[CAg-H_2O]^+$-4 and $[CAg-H_2O]^+$-5 correspond to a water molecule acting as a hydrogen bond acceptor with the N(1)-H bond, and
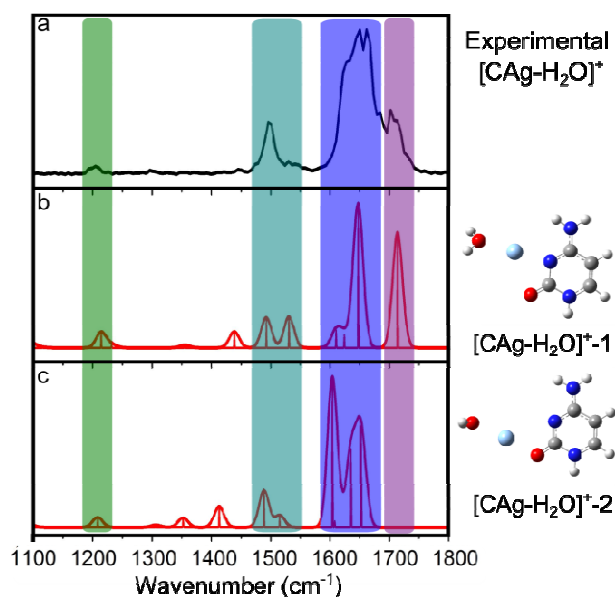
the N(8)-H of the amino group, respectively. These structures are predicted to be high in energy and should not be populated under our experimental conditions.

Table 2. Most stable isomers of the [CAg-H$_2$O]$^+$ complex. The potential energy surface was explored at the B3LYP level of theory using the 6-311G++(d,p) basis set for the C, H, N and O atoms and the Stuttgart effective core potential for Ag.[41] Thermochemical properties have been computed at 300K taking in to account the zero point correction, R.P. stands for relative population. All the values are expressed in eV.

	[CAg-H$_2$O]$^+$-1	[CAg-H$_2$O]$^+$-2	[CAg-H$_2$O]$^+$-3
ΔH (0 K)	0	0.02	0.38
ΔG (300 K)	0.01	0	0.43
Relative Population (R.P.)	0.6 (38 %)	1.0 (62 %)	6.7x10^{-8}

	[CAg-H$_2$O]$^+$-4	[CAg-H$_2$O]$^+$-5
ΔH (0 K)	0.48	0.51
ΔG (300 K)	0.48	0.52
Relative Population (R.P.)	9.0x10^{-9}	1.6x10^{-9}

The experimental IRMPD spectrum of $[CAg-H_2O]^+$ is given in Figure 4 along with the predicted IR absorption spectra of the two most stable $[CAg-H_2O]^+$-1 and $[CAg-H_2O]^+$-2 isomers which could be populated.

Figure 4. a) Experimental IRMPD spectrum of $[CAg-H_2O]^+$ complex. (b and c) Simulated IR absorption spectra of $[CAg-H_2O]^+$ -1 and $[CAg-H_2O]^+$ -2 isomers respectively.

The minor feature of the experimental IRMPD spectrum peaking at 1215 cm^{-1} (green rod) is observed in both simulated spectra around 1211 cm^{-1} and corresponds to an in-plane aromatic CCH bending mode. The second group of bands (light blue rod) peaking at 1511 cm^{-1} in the experimental spectrum, could be originated by the overlapping of two bands associated with the C-C bond deformation, that are predicted at 1490 cm^{-1} and 1515 cm^{-1} for the $[CAg-H_2O]^+$-1 isomer, and at 1490 cm^{-1} and 1533 cm^{-1} for the of $[CAg-H_2O]^+$-2 isomer.
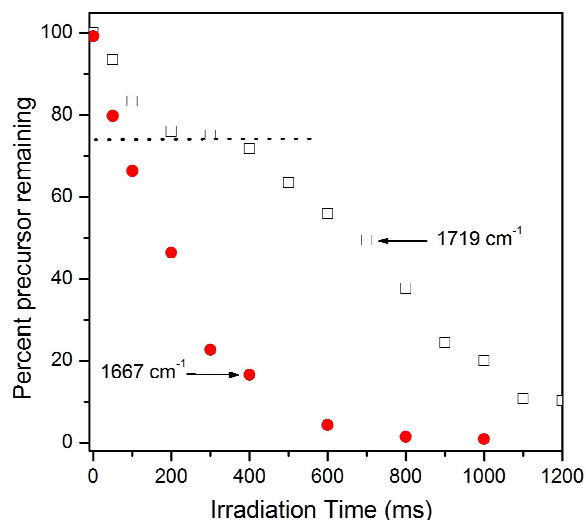
The higher energy part of the spectrum is the most structurally diagnostic. The band appearing at 1719 cm^{-1} is a clear IR signature a carbonyl stretching mode of the $[CAg-H_2O]^+$-1 isomer which is predicted at 1715 cm^{-1} (Figure 4.b, violet rod). If only this $[CAg-H_2O]^+$-1 isomer was populated, a narrow

band would be expected on the red-side of this free carbonyl stretch on resonance with the NH_2 scissoring mode of the $[CAg-H_2O]^+$-1 isomer predicted at 1648 cm^{-1}. The fact that a broad band centered at 1667 cm^{-1} with an intense shoulder at 1639 cm^{-1} (blue rod) is observed, strongly suggests that the $[CAg-H_2O]^+$-2 isomer is also populated under our experimental conditions. Due to the coordination to Ag^+, the $[CAg-H_2O]^+$-2 carbonyl stretching is predicted to be red shifted by 133 cm^{-1}, appearing at 1602 cm^{-1}. Therefore the maximum of the broad band at 1667 cm^{-1} with an intense shoulder at 1639 cm^{-1} could be interpreted considering that the two $[CAg-H_2O]^+$-1 and $[CAg-H_2O]^+$-2 isomers have NH_2 scissoring modes predicted at the same frequencies, and the presence of the shoulder at 1639 cm^{-1} may be assigned to the red shifted carbonyl stretching mode of the $[CAg-H_2O]^+$-2 isomer.

This interpretation of the IRMPD spectrum would be consistent with the predicted relative Boltzmann populations calculated at 300 K (Table 2). Providing that isomer-specific bands are observed, IRMPD kinetic measurements can also be useful to disentangle the co-existence of various isomers and experimentally determine their relative population.[48] This approach could thus be used in the present case assuming that the 1719 cm^{-1} band is a signature of free-carbonyl containing isomers. The kinetics of the depletion of the parent ions was thus recorded with the laser tuned at 1719 cm^{-1}. The results are shown in Figure 5, along with the results obtained when the laser was tuned at 1667 cm^{-1}, *i.e.* at a wavenumber where both the $[CAg-H_2O]^+$-1 and $[CAg-H_2O]^+$-2 isomers are predicted to have a strong IR absorption band.

As expected, irradiation at 1667 cm^{-1} shows a single exponential decay behavior. Upon irradiation at 1719 cm^{-1}, however, an inflection point at $\sim$ 74 % of the intensity which corresponds to $\sim$ 26 % depletion of the parent ion is observed in Figure 5. This observation supports the hypothesis of the formation of the $[CAg-H_2O]^+$-1 and $[CAg-H_2O]^+$-2 isomers. A fast dissociation of the former, which has a free carbonyle stretch, is expected at 1719 cm^{-1}, whereas the remaining $[CAg-H_2O]^+$-2 population
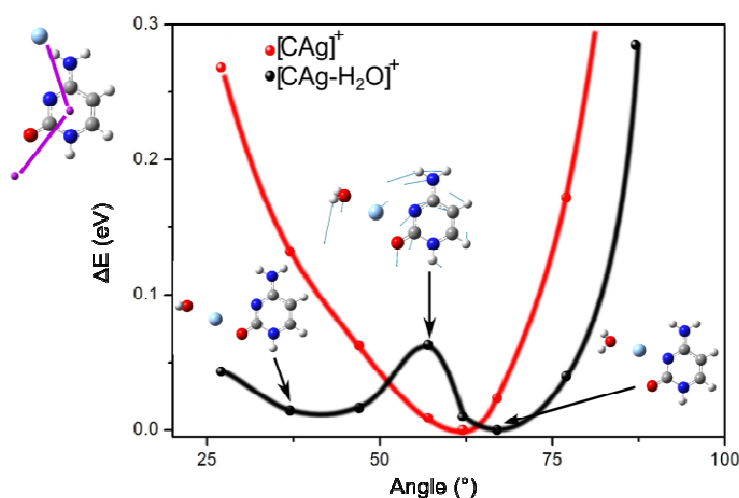
dissociates much more slowly due to off-resonance absorption or slow interconversion to the [CAg-H$_2$O]$^+$-1 isomer, from which it can absorb photons to reach the dissociation limit.

Figure 5: IRMPD kinetics for the [CAg-H$_2$O]$^+$ complex at 1667 cm^{-1} (red filled circles) and 1719 cm^{-1} (black open squares). The dashed line indicates the inflection point.

From these kinetic measurement, it is estimated that 26 % of the total population is due to the [CAg-H$_2$O]$^+$-1 isomer and the remaining 74 % adopts the [CAg-H$_2$O]$^+$-2 structure. These values are in close agreement with the theoretical prediction of 38 % and 62 %, respectively (Table 2). The relative ΔG(300K) determined from the experimental populations obtained from the IRMPD kinetic measurements is 2,6 kJ/mol (0.027 eV), in relatively good agreement with the theoretical value of 0.01 eV reported in Table 2. It should be noted, that both theory and experiment agree with the fact that the relative energies of the two types of structure is small, and that both isomers should be populated at room temperature assuming a Boltzmann population.

To evaluate the existence of the two energy wells in the potential energy surface and to estimate the height of the energy barrier between them, a relaxed scan of the angle established between Ag$^+$ and two ghost atoms (see Figure 6) was performed for the [CAg-H$_2$O]$^+$ complex.

Figure 6. Potential energy curve along the isomerization coordinate obtained from a relaxed scan of this coordinate which is described by the angle established between Ag^+ and two ghost atoms (pink atoms in the structure on the left of the figure). In black is shown the potential energy curve for the isomerization of the $[CAg-H_2O]^+$ complex and in red for the $[CAg]^+$ complex. Insert are the structures of the energy minima and the transition state for the isomerization of the $[CAg-H_2O]^+$ complex.

As can be seen in Figure 6, the two minima are separated by a low-energy barrier of 0.05 eV with respect to isomer $[CAg-H_2O]^+$-2. The transition state (TS) for the isomerization has an imaginary frequency of $i60.3$ cm^{-1} (7.5 x 10^{-3} eV) which is much lower than the isomerization energy barrier. Considering that under the experimental conditions (300 K) the average thermal energy (0.024 eV) is below the energy barrier, most of the population of both isomers is trapped in their potential wells and only a small fraction with enough thermal energy, in the tail of the Boltzmann distribution, can isomerize. Therefore, upon irradiation at 1719 cm^{-1} on the resonant band of the $[CAg-H_2O]^+$-1 isomer, a fast depletion of the ions is observed at short irradiation times. Then, there is an induction period until the $[CAg-H_2O]^+$-2 isomer can establish a steady state for the interconversion of the highest energy fraction of the thermal distribution.
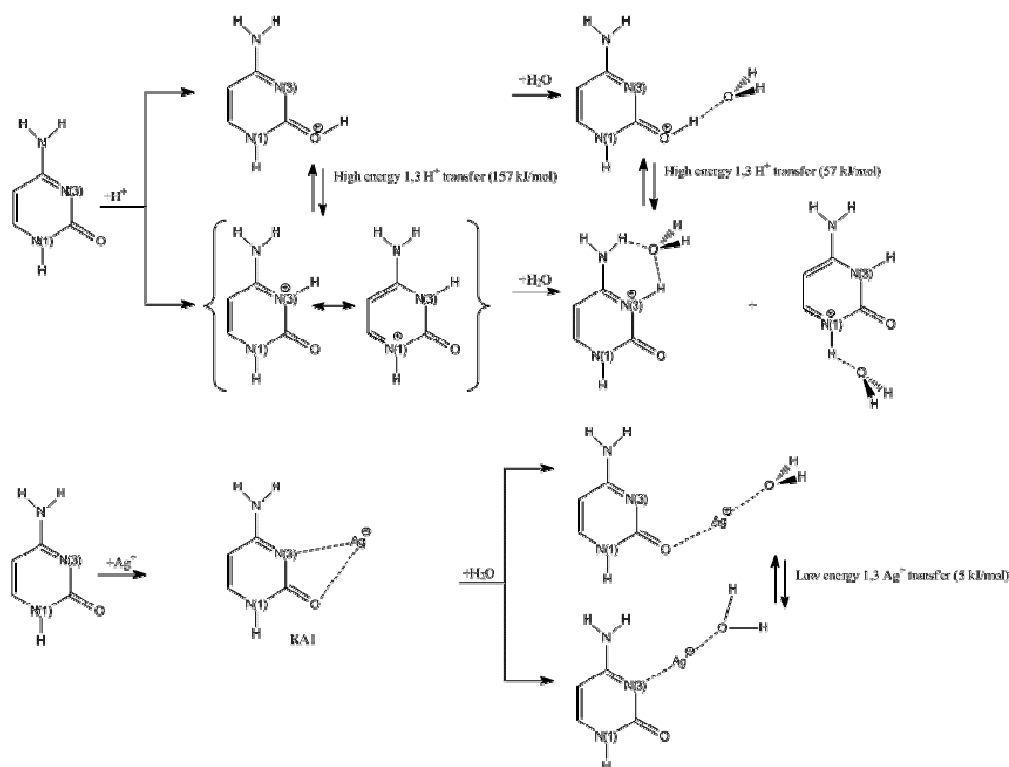
The same relaxed scan has been performed for the [CAg]$^+$ complex (Figure 6). Interestingly, the position of Ag$^+$ in the energy minimum along the reaction coordinate (62°) is very close the position TS structure for the isomerization of the [CAg-H$_2$O]$^+$ complex.

A tentative interpretation of this water induced change of the shape of the potential energy surface can be proposed based on the propensity of Ag$^+$ to form linear di-coordinated complexes. It is well known that upon formation of a first Ag$^+$-ligand bond defining the z-axis, s-dσ hybridization occurs in order to reduce the electron density along the z-axis.[47] As a consequence, the second ligand binds opposite to the first, leading to a linear di-coordinated Ag$^+$ complex. This phenomenon has been observed for gas phase Ag$^+$ complexes.[37,46,47] When Ag$^+$ interacts with only one cytosine molecule as in the case of the [CAg]$^+$ complex, there is no possibility to form linear complex and Ag$^+$ binds to two functional groups as in the KA1 lowest energy structure. Upon addition of water, however, as in the case of the [CAg-H$_2$O]$^+$ complex, the most favorable linear configuration can be adopted, with the Ag$^+$ interacting on one side with one of the electron donating groups of cytosine and on the other side with the oxygen atom of the water molecule.

A comparison between [CH]$^+$ and [CAg]$^+$ and their corresponding monohydrated complexes is given in Scheme 1. While protonation of cytosine lead to two stable KA and EA tautomers separated by a high energy barrier (157 kJ/mol), interaction with Ag$^+$ leads to a single KA tautomer as previously predicted,[32,45] that favors the electrostatic interaction of the cation with the negative density charge on N(3) and C(2)=O(7), which is possible given the larger size of Ag$^+$ as compared to H$^+$.

The interaction of a single water molecule with [CH]$^+$ or [CAg]$^+$ complexes is determined to take place on the H$^+$ or Ag$^+$ cations, respectively. In the case of [CH-H$_2$O]$^+$ it has been shown that H$_2$O catalyzes the 1,3 proton transfer/isomerization reaction reducing the barrier from 157 kJ/mol to 57 kJ/mol.[10,12] On the contrary, in the case of [CAg-H$_2$O]$^+$ the water molecule allows stabilization of two

isomers in a linear coordination geometry and as a consequence a very low energy barrier (5 kJ/mol) for

the isomerization is developed.

Scheme 1: comparison of the [CH]$^+$ and [CAg]$^+$ complexes and their mono-hydrated complexes.

The fact that two almost iso-energetic isomers can be produced is undesirable for using this

type of interactions for synthesizing non-conventional DNAs because the lack of specificity in the

interaction could lead to fails in the replication process. However, while Ag$^+$…cytosine interaction is not-

specific in the linear di-coordinated [CAg-H$_2$O]$^+$ complex, in the case of the metal mediated base pair

[C$_2$Ag]$^+$ only one isomer was found. In this structure the interaction of Ag$^+$ with both cytosine molecules

takes place on N(3).[37] This is a consequence of the additional stabilization of the base pair through a H-

bond between both cytosine molecules, which is not feasible when Ag$^+$ interacts on one of C(2)=O(7)

groups. Therefore, the preferential stabilization of a single isomer in metal-mediated base pairs such

[C$_2$Ag]$^+$, could be considered as a signature of an expected higher fidelity in the replication process of DNA molecules containing these type of interactions.

4. Conclusions

By combining mass selected IRMPD spectroscopy with theoretical calculations, the structures of the [CAg]$^+$ and [CAg-H$_2$O]$^+$ complexes were determined. While only one isomer with cytosine in the keto-amino (KA) form and Ag$^+$ interacting simultaneously with the O(7) atom of the C(2)=O(7) group and N(3) was clearly observed for the [CAg]$^+$ complex, mono-hydration of this complex stabilizes two quasi-isoenergetic isomers in the [CAg-H$_2$O]$^+$ complex. In the later complex, Ag$^+$ is bound to the O atom of the water molecule and either to N(3) or C(2)=O(7) group in each isomer with a linear geometry (e.g. the H$_2$O-Ag$^+$-N(3) and H$_2$O-Ag$^+$-C(2)=O(7) angles equal to 180°) in both cases.

Comparison of these results with those of protonated cytosine and its mono-hydrated complex, indicates that the larger size of Ag$^+$ as compared to H$^+$ allows its simultaneous interaction with N(3) and C(2)=O(7) while it is not possible for the case of H$^+$ and then it interacts in two well defined leading to two isomers. On the other hand, while a single water molecule catalyzes the isomerization reaction in the case of [CH-H$_2$O]$^+$, it stabilizes two different isomers in the case of [CAg-H$_2$O]$^+$ and develops a small energy barrier between them.

Acknowledgments

Notes and References

1) F. Crick, *Nature*, 1970, **227**, 561-563.

2) B. Lippert and D. Gupta, *Dalton Trans.*, 2009, 4619-4634.

3) B. Lippert, *Coord. Chem. Rev.,* 2000, **200-202**, 487-516.

4) Y. Takezawa and M. Shionoya, *Acc. Chem. Res.,* 2012, **45**, 2066-2076

5) K. S. Park, C. Jung, H. G. Park, *Angew. Chem. Int. Ed.*, 2010, **49**, 9757-9760.

6) S. Liu, G. H. Clever, Y. Takezawa, M. Kaneko, K. Tanaka, X. Guo and M. Shionoya, *Angew. Chem. Int. Ed.*, 2011, **50**, 8886 – 8889.

7) Z. Kukenyik and L. G. Marzilli. *Inorg. Chem.* 1996, **35**, 5654 -5662.

8) A. Ono, C. Shiqi, T. Humika, M. Tashiro, T. Fujimoto, T. Machinami, S. Oda, Y. Miyake, I. Okamoto and Y. Tanaka, *Chem. Commun.*, 2008, **44**, 4825 – 4827.

9) H. Urata, E. Yamaguchi, Y. Nakamura and S. Wada, *Chem. Commun.*, 2011, **47**, 941 – 943.

10) J. Y. Salpin, S. Guillaumont, J. Tortajada, L. MacAleese, J. Lemaire and P. Maitre, *ChemPhysChem*, 2007, **8**, 2235 – 2244.

11) J. M. Bakker, R. K. Sinha, T. Besson, M. Brugnara, P. Tosi, J. Y. Salpin and P. Maitre, *J. Phys. Chem. A*, 2008, **112**, 12393 – 12400.

12) J. M: Bakker, Y. Y. Salpin and P. Maitre, *Int. J. Mass. Spectrom.*, 2009, **283**, 214 – 221.

13) M. Berdakin, G. Féraud, C. Dedonder-Lardeux, C. Jouvet and G. A. Pino, *Phys. Chem. Chem. Phys.*, 2014, **16**, 10643 – 10650.

14) N. R. Cheong, S. H. Nam, H. S. Park, S. Ryu, J. K. Song, S. M. Park, M. Pérot, B. Lucas, M. Barat, J. A. Fayeton and C. Jouvet, *Phys. Chem. Chem. Phys.*, 2011, **13**, 291 – 295.

15) S. Ovad Pedersen, K. Stochkel, C. Skinnerup Byskov, L. Munksgaard Baggesen and S. Bronsted Nielsen, *Phys. Chem. Chem. Phys.*, 2013, **15**, 19748 – 19752.

16) G. Féraud, C. Dedonder-Lardeux, C. Jouvet, Y. Inokuchi, T. Haino, R. Sekiya and T. Ebata, *J. Phys. Chem. Lett.*, 2014, **5**, 1236 -1240.

17) B. Yang, R. R. Wu, G. Berde, J. Oomens and M. T. Rodgers, *J. Phys. Chem. B*, 2013, **117**, 14191 – 14201.

18) G. Féraud, M. Berdakin, C. Dedonder-Lardeux, C. Jouvet and G. A. Pino, *J. Phys. Chem. B*, 2014, **119**, 2219 – 2228.

19) B. Yang and M. T. Rodgers, *J. Am. Chem. Soc*. 2013, **136**, 282 – 290.

20) J. Oomens, A. R. Moehlig, T. H. Morton, *J. Phys. Chem. Lett.*, 2010, **1**, 2891 – 2897.

21) B. Yang, A. R. Moehlig, C. E. Frieler and M. T. Rodgers, *J. Phys. Chem. B*, 2015, **119**, 1857–1868.

22) H. Kang, G. Féraud, C. Dedonder-Lardeux and C. Jouvet, *J. Phys. Chem. Lett.*, 2014, **5**, 2760 – 2764.

23) B. Yang, R. R. Wu, N. C. Polfer, G. Berden, J. Oomens, and M. T. Rodgers, *J. Am. Soc. Mass Spectrom*, 2013, **24**, 1523–1533.

24) C. M. Kaczan, A. I. Rathur, R. R. Wu, Y. Chen, C. A. Austin, G. Berden, J. Oomens and M.T. Rodgers, *Int. J. Mass Spectrom.*, 2015, **378**, 76–85.

25) J. Y. Salpin, S. Guillaumont, D. Ortiz, J. Tortajada and P. Maitre, *Inorg. Chem.* 2011, **50**, 7769 – 7778.

26) J. Y. Salpin, L. Gamiette, J. Tortajada, T. Besson and Philippe Maitre, *Int. J. Mass. Spectrom.* 2011, **304**, 154-164.

27) G. Chiavarino, M. E. Crestoni, S. Fornarini, D. Scuderi adn J. Y. Salpin, *J. Am. Chem. Soc.*, 2013, **135**, 1445 – 1455.

28) J. Y. Salpin, L. MacAleese, F. Chirot and P. Dugourd**,** *Phys. Chem. Chem. Phys.*, 2014, **16**, 14127-14138.

29) Y. Nosenki, F. Memges, C. Riehn, G. Niedner-Schatteburg, *Phys. Chem. Chem. Phys.*, 2013, **15**, 8171 – 8178.

30). M. V. Vázquez and A. Martínez, J. Phys. Chem. A, 2007, 111, 9931-9939.

31) J. Valsespino-Saenz and A. Martínez, J. Phys. Chem. A, 2008, 112, 2408 – 2414.

32) M. V. Vázquez and A. Martínez, J. Phys. Chem. A, 2008, 112, 1033 – 1039.

33) P. Sharma, H. Singh, S. Sharma and H. Singh, J. Chem. Theory Comput., 2007, 3, 2301 – 2311.

34) A. Martínez, J. Phys. Chem. A, 2009, 113, 1134 – 1140.

35) G. Lv, F. Wei, H. Jiang, Y. Zhou and X. Wang, J. Molec. Struct. Theochem, 2009, 915, 98 – 104.

36) P. Sharma, S. Sharma, A. Mitra and H. Singh, J. Biom. Struct. Dyn., 2009, 27, 65 - 81.

37) M. Berdakin, V. Steinmetz, P. Maitre and G. A. Pino, *J. Phys. Chem. A*, 2014, **118**, 3804 – 3809.

38) H. A. Day, C. Huguin and Z. A. E. Waller, *Chem. Commun.,* 2013, **49**, 7696 -7698.

39) M. Berdakin, G. Féraud, C. Dedonder-Lardeux, C. Jouvet and G. A. Pino, *J. Phys. Chem. Lett.*, 2014, **5**, 2295 – 2301.

40) J. M. Bakker, T. Besson, J. Lemair, D. Scuderi and P. Maitre, *J. Phys. Chem. A*, 2007, **111**, 13415 – 13424.

41) D. Andrea, U. Houssermann, M. Dolg, M. Stoll and H. Preuss, *Theor. Chim. Acta*, 1990, **77**, 123 – 141.

42) H. H. Ritze and W. Radloff, *Chem. Phys. Lett.*, 1996, **250**, 415 – 420.

43) O. Hernández, B. Paizs and P. Maitre, *Int. J. Mass. Spectrom.*, 2015, **377**, 172 – 178.

44) M. J. Frisch, G. W. Trucks, H. B. Schlegel, G. E. Scuseria, M. A. Robb, J. R. Cheeseman, G. Scalmani, V. Barone, B. Mennucci, G. A. Petersson, H. Nakatsuji, M. Caricato, X. Li, H. P. Hratchian, A. F. Izmaylov, J. Bloino, G. Zheng, J. L. Sonnenberg, M. Hada, M. Ehara, K. Toyota, R. Fukuda, J. Hasegawa, M. Ishida, T. Nakajima, Y. Honda, O. Kitao, H. Nakai, T. Vreven, J. A. Montgomery, J. E. Peralta, F. Ogliaro, M. Bearpark, J. J. Heyd, E. Brothers, K. N. Kudin, V. N. Staroverov, R. Kobayashi, J. Normand, K. Raghavachari, A. Rendell, J. C. Burant, S. S. Iyengar, J. Tomasi, M. Cossi, N. Rega, N. J. Millam, M. Klene, J. E. Knox, J. B. Cross, V. Bakken, C. Adamo, J. Jaramillo, R. Gomperts, R. E. Stratmann, O. Yazyev, A. J. Austin, R. Cammi, C. Pomelli, J. W. Ochterski, R. L. Martin, K. Morokuma, V. G. Zakrzewski, G. A. Voth, P. Salvador, J. J. Dannenberg, S. Dapprich, A. D. Daniels, Ö. Farkas, J. B. Foresman, J. V Ortiz, J. Cioslowski, and D. J. Fox, 2009.

45) P. H. Acioli and S. Srinivas, *J. Molec. Model*., 2014, **20**, 2391.

46) S. Chakraborty and O. Dopfer, *ChemPhysChem*, 2011, **12**, 1999 – 2008.

47) H. Koizumi, M. Larson, F. Muntean, P. B. Armentrout, *Int. J. Mass Spectrom.*, **2003**, 228, 221 -235.

48) J. S. Prell, T. M. Chang, J. A. Biles, G. Berden, J. Oomens and E. R. Williams, *J. Phys. Chem. A*, 2011, **115**, 2745 – 2751.